https://doi.org/10.1142/9789811280184_0004

Chapter 4

Physics Results

Albert De Roeck*, Monica Pepe Altarelli* and Pierre Savard†

*CERN, Geneva, Switzerland

†University of Toronto, Toronto, Canada and TRIUMF, Vancouver, Canada

1. Introduction

On the 23rd November 2009, the LHC came alive for the experiments with first proton-proton collisions delivered for physics at the beam injection energy, i.e., for a centre of mass (CM) energy, $\sqrt{s}$, of 900 GeV. On the 30th of November the beam energy was ramped-up to 1.18 TeV, thus setting the world record for highest energy particle collider in the world at $\sqrt{s}$ = 2.36 TeV, beating the Tevatron at FNAL by a narrow margin.

The LHC started its first real high-energy run on March 30th 2010 with the beam energy ramped-up to 3.5 TeV, leading to proton-proton collisions with $\sqrt{s}$ = 7 TeV, and which was the start of the exploration of a new energy regime for fundamental physics. The event was extensively covered by the popular media, and the particle physics community was particularly excited by this groundbreaking event. In particular the experiments demonstrated they were ready for the much anticipated physics data run. Experiments at the LHC collider that have collected data since then are the "high luminosity" general purpose detectors ATLAS[1] and CMS,[2] the heavy-flavor experiment LHCb,[3] the heavy ion experiment ALICE,[4] two forward detectors TOTEM[5] and LHCf[6] and the Monopole and Exotica search detector MoEDAL.[7]

The LHC continued its operation at $\sqrt{s}$= 7 TeV in 2011 and increased the CM energy to 8 TeV in 2012, the last year of run 1. The integrated

luminosity collected by the experiments increased rapidly in the these first years. E.g., CMS collected 36 pb^{-1}, 5 fb^{-1}, and about 20 fb^{-1} in 2010, 2011 and 2012, respectively.

Run 2 started in 2015 after a two-year shut-down and partial upgrade of the LHC machine. The beam energy for this run was raised to 6.5 TeV, close to the maximum nominal beam energy value of 7 TeV. Hence, $\sqrt{s}$ in run 2 was 13 TeV, and opened a new window for searches of new physics (NP) and precision measurements at the energy frontier. After the exploratory 2015 run, the main part of the integrated luminosity was collected in the years 2016–2018 with a total of about 140 fb^{-1} each, for ATLAS and CMS. Collecting data at increasingly higher instantaneous luminosity led to having more proton-proton collisions within one bunch crossing of the beams, so called pileup collisions. The average number of pileup interactions was 23 (32) in 2016 (2017–2018). LHCb takes data at a lower instantaneous luminosity to reduce the impact of pileup events, and has collected a total integrated luminosity of 3 fb^{-1} (6 fb^{-1}) in run 1 (run 2).

2. QCD measurements

Hadrons consist of partons, which carry the charge of the strong force. Collisions involving high p_T phenomena can be treated in a perturbative way. But by far most hadronic collisions at the LHC are so called soft collisions in the non-perturbative regime.

The TOTEM collaboration, using forward detectors and a proton spectrometer integrated with the beampipe, has measured elastic, inelastic, diffractive and total cross-section at the available LHC CM energies to date.[8] The pp total cross section is measured in a range from $\sqrt{s}$ = 2.76 TeV to 13 TeV, obtaining a variation from (84.7 ± 3.3) mb to (110.6 ± 3.4) mb, and the nuclear slope B of the elastic scattering is measured to be (20.36 ± 19) GeV^2 at the highest collision energy. During run 2 TOTEM and CMS jointly built a new proton spectrometer and now produce common physics studies (see, e.g. Ref. 9).

The precision of TOTEM allowed showing evidence for a non-exponential elastic proton–proton differential cross-section at low $|t|$ at 8 TeV.[10] Another important result of TOTEM, made recently by combining results with the D0 experiment at FNAL, is the first observation of Odderon exchange, from the elastic scattering differences between proton-proton and proton–antiproton data.[11]

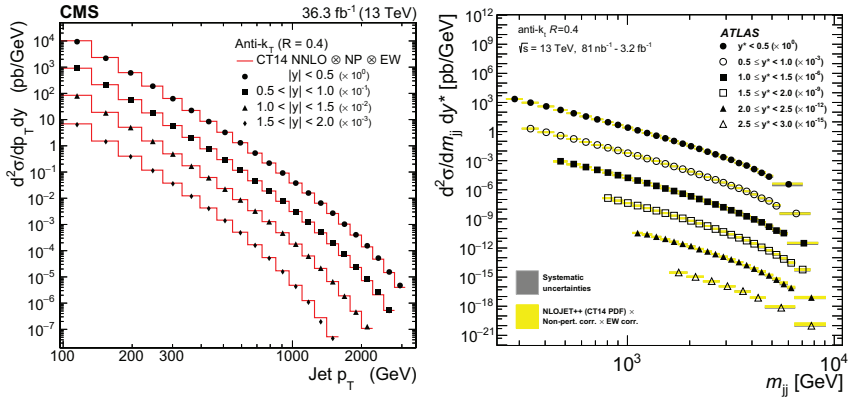

Fig. 1. (Left) The inclusive jet production cross sections as a function of the jet transverse momentum p_T measured in intervals of the absolute rapidity $|y|$. The cross section obtained for jets clustered using the anti-k_T algorithm with R = 0.4 is shown. The measurements are compared with fixed-order NNLO QCD predictions (solid line) using CT14nnlo PDF and corrected for electroweak and non-perturbativce effects. From Ref. 18. (Right) Dijet cross-sections as a function of m_{jj} and $y^* = |y_1 - y_2|/2$, for anti-k_T jets with R = 0.4. The dark gray shaded areas indicate the experimental systematic uncertainties. The data are compared to NLO pQCD predictions calculated using NLOJET++ with $p_T^{max}\exp(0.3y^*)$ as the QCD scale and the CT14 NLO PDF set, to which non-perturbative and electroweak corrections are applied. The light yellow shaded areas indicate the predictions with their uncertainties. From Ref. 19.

The LHCf experiment is designed to measures the very forward, at zero degrees, emitted neutral particles, namely neutrons and π^0s/photons, with the goal to test Monte Carlo (MC) models that are used for cosmic ray interaction studies. The LHCf data showed important deficiencies of the presently used MC models,[12,13] and was used to improve them. ALICE, ATLAS, CMS and LHCb have all made detailed measurements on particle multiplicities in soft collisions. In fact the first physics papers produced at the LHC were soft QCD measurements with the data from the initial short run at 900 GeV.[14–17]

The success of perturbative QCD has been demonstrated most convincingly with the measurements of inclusive jet cross sections for jet p_T up to and above 2 TeV. Results for the double-differential jet p_T and di-jet mass cross sections are shown in Fig. 1.[18,19] The QCD calculations shown in the figures describe the cross sections of the data over more than nine orders of magnitude.

Perturbative QCD measurements can be used to derive information on

the strong force e.g., the strong coupling constant α_s and on the parton distributions functions (PDFs) of the proton. PDFs are key ingredients in predicting cross sections of all processes at a hadron collider, and are traditionally extracted from experimental data such as lepton-hadron scattering. In recent years perturbative QCD data from hadron colliders have emerged as important information to extract PDFs, as, e.g., demonstrated in Ref. 18. Most recent studies of PDFs use Tevatron and LHC jet data in general PDF fits (see, e.g. Ref. 20), demonstrating their power to constrain, e.g, the gluon distribution in the proton.

The strong coupling constant has been measured using various methods: inclusive jet measurements, ratios from 3-jet to 2-jet events (R32), 3-jet mass measurements, top production, transverse energy correlations and more. As an example, the R32 method gives $\alpha_s(m_Z) = 0.1148 \pm 0.0014_{\rm exp} \pm 0.0018_{\rm PDF} \pm 0.0050_{\rm theory}$. Currently, the most precise $\alpha_s(m_Z)$ derivation from LHC data is that from inclusive W and Z cross sections[21] with about 1.6% uncertainty.

QCD data at the LHC are now used to make detailed jet and multi-jet, forward jet, and photoproduction studies and to address more physics topics, probing with increasing accuracy the perturbative QCD regime.

3. Electroweak measurements

The ATLAS and CMS detectors were designed to make high precision measurements of electrons, muons, and missing transverse momentum in the harsh high luminosity environment of the LHC. This level of performance coupled with the large data samples available after a decade of running, has resulted in measurements of electroweak observables at a precision that is now surpassing that of previous lepton colliders. In addition, the study of multi-boson final states now includes previously unmeasured processes that involve the quartic couplings of the SM. These measurements, in concert with those associated with the Higgs boson, provide numerous opportunities to test the electroweak sector of the SM.

The precision of W mass measurements at hadron colliders has now surpassed that achieved at LEP. The ATLAS collaboration has reported results with an uncertainty of 19 MeV[22] and the LHCb collaboration has achieved a total uncertainty of 32 MeV,[23] dominated by statistics, based on about a third of the collected data. The fact that the LHCb experiment has reported a precision measurement of the W boson mass is remarkable, considering the limited angular acceptance and lower instantaneous luminosity

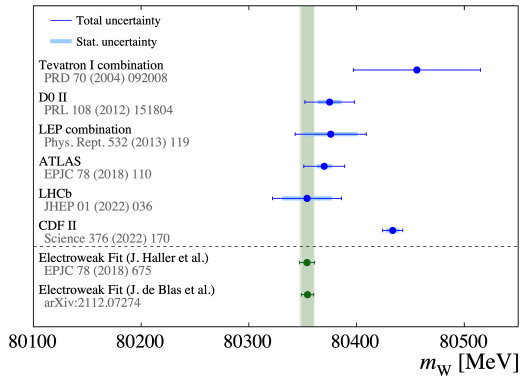

Fig. 2. W boson mass measurements from LEP, LHC, and Tevatron experiments compared with the SM expectation.[24]

of the experiment. The LHCb measurement features many systematic uncertainties that are mostly uncorrelated with those of ATLAS and CMS, which will be helpful in future combinations. A comparison with other experiments, including the latest result from CDF, is shown in Fig. 2. Improved results using run 2 data are expected from all experiments in the future.

The Weinberg angle (θ_W) is another central electroweak parameter that has been measured at the LHC. ATLAS, CMS, and LHCb have measured the value of $\sin^2(\theta_W)$ with a precision of 0.00036,[25] 0.00053,[26] and 0.00106,[27] respectively. The largest source of systematic uncertainty is associated with PDFs.

Weak boson production has been extensively studied by the LHC experiments over more than a decade. Precision measurements of single W and Z production, and of diboson production were performed during run 1 and run 2 at CM energies of 7, 8, and 13 TeV. With the larger datasets made available in run 2, more rare multi-boson production processes could also be investigated. This includes vector boson scattering measurements and triboson production measurements (see Fig. 3). Vector boson scattering has now been observed at the LHC in the WW, WZ, ZZ, $Z\gamma$ final states.

4. Flavour physics

The comprehensive program of flavour studies realized at the LHC, in particular by the LHCb experiment, has demonstrated that the LHC is an ideal

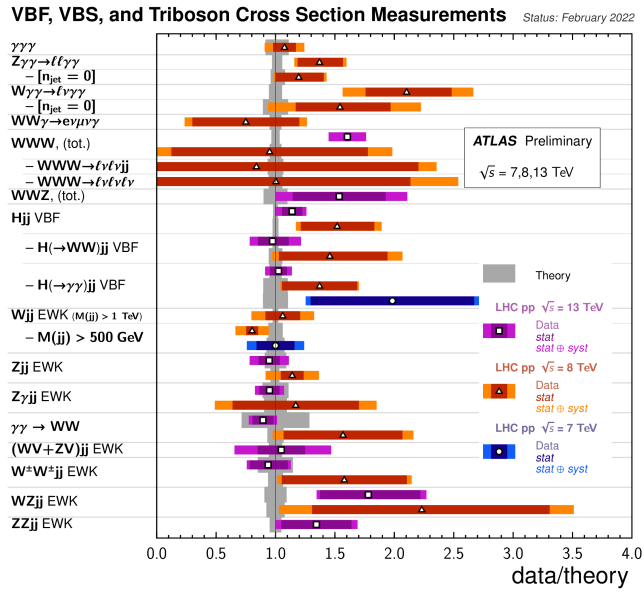

Fig. 3. Vector boson scattering, vector boson fusion, and triboson production measurements performed by the ATLAS experiment[28] and compared with the SM expectation.

laboratory for flavour physics. Much interest is devoted to rare b-hadron decays mediated by flavour-changing neutral currents (FCNC). In the SM these decays are forbidden at tree level but can occur at loop level; a new particle too heavy to be produced at the LHC can still give sizeable effects when exchanged in a loop, thus providing sensitivity to shorter distances or effectively higher energies. This is an indirect strategy to NP searches, which nicely complements direct searches performed by ATLAS and CMS and is particularly relevant in the absence of direct collider production of new particles. The baryon asymmetry of the universe needs CP violation far beyond that provided by the SM. Precision measurements of the Cabibbo-Kobayashi-Maskawa (CKM) matrix elements and searches for possible inconsistencies in measurements of the angles and sides of the unitarity triangles probe the CKM description of flavour-changing processes and the mechanism of CP violation through the phase in the quark-mixing matrix. Heavy-flavour physics also provides a unique laboratory for studying the strong interaction. Many hadrons with nonstandard quantum numbers that contain charm or beauty quarks have been discovered at the LHC, opening up a very active area of hadronic-physics research.

4.1. *Rare B-meson decays and flavour anomalies*

The study of rare decays is central to the LHC flavour program providing a wealth of opportunities, including in charm and strange decays. The decay $B^0_{(s)} \to \mu^+\mu^-$ has been identified as a very interesting potential constraint on the parameter space of NP models and is one of the milestones of the flavour program. Within the SM, this decay is very rare as it is a FCNC process with helicity and CKM suppression. Theoretically, it is reliably and precisely predicted,[29,30] with branching fractions $\mathcal{B}(B^0_s \to \mu^+\mu^-) = (3.66 \pm 0.14) \times 10^{-9}$ and $\mathcal{B}(B^0 \to \mu^+\mu^-) = (1.03 \pm 0.05) \times 10^{-10}$. This decay is also characterized by a very clean experimental signature and it has been studied by all high-energy collider experiments in an effort that lasted almost forty years. Experiments at the LHC have taken the lead in the analysis of these decays, profiting from the very large B-meson cross-section and their excellent muon reconstruction and identification. The combination of the ATLAS, CMS and LHCb measurements using data collected between 2011 and 2016 gives $\mathcal{B}(B^0_s \to \mu^+\mu^-) = (2.69^{+0.37}_{-0.35}) \times 10^{-9}$ and no significant signal for $B^0 \to \mu^+\mu^-$, leading to an upper limit of 1.9×10^{-10} at 95% confidence level (CL).[31] The two-dimensional compatibility with the SM point is 2.1 σ (see Fig. 4, left). A recent CMS update[32] based on the full run 1 and run 2 data, provides the most precise measurements to date, which are fully consistent with the SM, thus reducing the overall tension. The CMS dimuon invariant mass distribution of the selected $B^0_{(s)} \to \mu^+\mu^-$ candidates in a region of high signal purity is shown in Fig. 4, right.

Much interest is devoted to exclusive semileptonic $b \to s\ell^+\ell^-$ transitions of the type $B \to H_s\mu^+\mu^-$, with H_s either a pseudoscalar or a vector meson. In many extensions of the SM, new particles can contribute to their amplitudes modifying the rates or angular distributions of the final-state particles. These decays are characterised by branching fractions of typically $\mathcal{O}(10^{-7})$, i.e., much larger than that of $B^0_{(s)} \to \mu^+\mu^-$. Contrary to the B-factory experiments, which exhibit similar efficiencies for muons and electrons, at the LHC measurements are performed in the dimuon final state, as muons can be triggered and reconstructed much more efficiently than electrons in the high-multiplicity hadronic environment. Measurements of the branching fractions are performed as a function of $q^2 = m^2_{\mu^+\mu^-}$, the dimuon invariant mass squared, to be able to exclude the regions around the J/ψ or the $\Psi(2S)$ resonances, where the rates are dominated by the tree-level decays $B \to H_s J/\Psi(\Psi(2S))$. The differential branching ratios $\mathrm{d}\mathcal{B}/\mathrm{d}q^2$ are measured in bins of q^2 and are compared to theoretical calculations

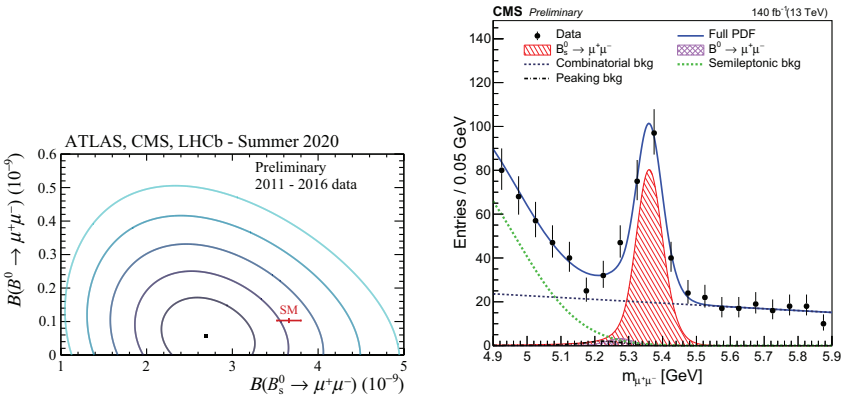

Fig. 4. (Left) Likelihood contours for the combination of ATLAS, CMS and LHCb in the plane $\mathcal{B}(B^0 \to \mu^+\mu^-)$ vs. $\mathcal{B}(B_s^0 \to \mu^+\mu^-)$ corresponding to 1 to 5 σ levels. The red point shows the SM prediction with its uncertainties. (Right) CMS invariant dimuon mass distribution of the selected $B^0_{(s)} \to \mu^+\mu^-$ candidates in a region of high signal purity (multivariate classifier>0.99); the result of the fit is overlaid (blue solid line) and the different background components are detailed in the caption.

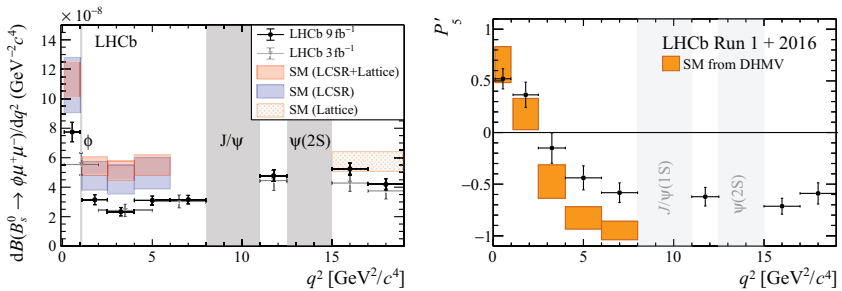

Fig. 5. (Left) Differential branching fraction $\mathrm{d}\mathcal{B}(B_s^0 \to \phi\mu^+\mu^-)/\mathrm{d}q^2$, overlaid with SM predictions using LCSR at low q^2,[37,38] and LQCD at high q^2.[39] The J/ψ and $\psi(2S)$ regions are vetoed in the selection of the signal mode. (Right) P'_5 observable as a function of q^2 measured by LHCb[40] and compared with SM calculations from Refs. 41,42.

generally based on Lattice Cone Sum Rules (LCSR) or Lattice QCD (LQCD). LHCb measured the differential branching fractions in several exclusive transitions.[33–36] As an example, Fig. 5, left, shows the differential branching fraction $\mathrm{d}\mathcal{B}(B_s^0 \to \phi\mu^+\mu^-)/\mathrm{d}q^2$,[36] overlaid with SM predictions using LCSR at low q^2,[37,38] and LQCD at high q^2.[39] In the q^2 region between 1.1 and 6.0 GeV$^2/c^4$, the measurement is found to lie 3.6 σ below a SM prediction based on a combination of LCSR and LQCD calculations.

Also for other exclusive decays, such as $B \to K^{(*)}\mu^+\mu^-$,[33,34] the branching fractions at low q^2 lie generally below the SM predictions, which are however affected by significant hadronic uncertainties.

Searches for NP can also be conducted from the analysis of the angular distributions of the final state particles in semileptonic $b \to s\ell^+\ell^-$ decays. Measuring angular distributions is particularly interesting because it is possible to construct optimised variables[43] that depend less on hadronic uncertainties associated with the transition form factors. A global fit performed by LHCb to several angular observables in $B^0 \to K^{*0}\mu^+\mu^-$ decays results in an overall tension with the SM of about 3 σ.[40] Figure 5, right, shows a comparison of the data with one such optimized observable, the so-called P_5' variable. A local discrepancy of about $2.5\,\sigma$ is measured in two bins in q^2. This discrepancy, however, should be taken with a grain of salt, given that there is no complete consensus about the theoretical uncertainty of the SM prediction.

LHCb has also performed tests of lepton flavour universality (LFU), which is a central property of the SM, looking for deviations from predictions in the ratios $R_H = \frac{B\to H\mu^+\mu^-}{B\to He^+e^-}$. Here, H denotes a K^+ or a K^{*0} (the so-called R_K and R_{K^*} ratios). These ratios are clean probes of NP because they are sensitive to new interactions that couple in a non-universal way to electrons and muons. They are also precisely calculated because hadronic uncertainties cancel in the ratios. In the SM, $R_H = 1$ neglecting lepton masses. The major challenge for this measurement stems from the markedly different detector response to electrons and muons, leading, e.g., to different trigger and reconstruction efficiencies, and background levels. Based on the total collected data, LHCb found deviations on R_K from LFU at $3.1\,\sigma$ for $q^2 \in [1.1, 6.0]\,\mathrm{GeV}^2/c^4$.[44] Deviations were also measured for R_{K^*}, based on the analysis of about one third of the sample,[45] namely $\sim 2.2\,\sigma$ for $q^2 \in [0.045, 1.1]\,\mathrm{GeV}^2/c^4$ and $\sim 2.5\,\sigma$ for $q^2 \in [1.1, 6.0]\,\mathrm{GeV}^2/c^4$.

Lepton universality tests are also performed using tree-level $b \to c$ transitions from the measurement of $R(D^{(*)}) = \frac{B(B\to D^{(*)}\tau\nu_\tau)}{B(B\to D^{(*)}\ell\nu_\mu)}$, with $\ell = \mu, e$. This enables a comparison between muons (or electrons) and tau leptons. A combination of $R(D)$ and $R(D^*)$ results from Belle, BaBar and LHCb is in tension with the SM at the $\sim 3.2\,\sigma$ level.[46]

Although not significant individually, these deviations have generated immense interest in the community because they can be interpreted coherently, leading to the exploration of new interesting theoretical avenues.

However, more recently, LHCb performed an improved, simultaneous

analysis of both R_K and R_{K^*} using the full dataset.[47,48] The two ratios were computed in two q^2 bins, thereby producing four independent measurements. This new analysis did not confirm the previous tensions and found results fully in line with the SM predictions. The main differences arise from a better understanding of misidentified hadronic backgrounds to the electron decay mode, determined at a tighter electron particle identification working point, and from the modelling of the residual hadronic backgrounds.

The search for deviations from the SM continues!

4.2. *Precision tests of the CKM framework*

The CKM matrix is able to describe a large range of phenomena with only four parameters, three angles and one phase, which is the only source of CP violation in the SM. The physics impact of the precise determination of these parameters is not so much in the determination of their absolute values, given that the CKM matrix is not predicted, but rather in testing the (in)consistency of the "ensemble" of measurements and how precisely the SM description of flavour and CP violation holds. Extensive measurements in K, D and B meson decays have been performed over the years by many different experiments, mostly at B factories, at the Tevatron and at the LHC, mainly by LHCb. At the current level of precision, all measurements are consistent and intersect in the apex of the unitary triangle, which geometrically describes the unitarity of the CKM matrix, indicating that NP effects can appear at most as small corrections to the CKM description.

The golden SM benchmark is the CKM angle γ, which can be determined with negligible theoretical uncertainty entirely from tree-level processes. Deviations between direct measurements of γ and the value derived from global CKM fits would be a clear indication of NP. Most measurements of γ utilize the fact that interference of $B^\pm \to D^0 K^\pm$ and $B^\pm \to \overline{D}^0 K^\pm$ can be studied in final states accessible in both D^0 and $\overline{D}^0$ decays. LHCb performed a combination of several complementary γ measurements that involve different intermediate neutral D-meson decays, including the LHCb run 2 update from the highly sensitive $B^\pm \to Dh^\pm$[49] with $D \to K^0_S h^+ h^-$, where $h^\pm$ is either a charged kaon or pion. From this combination, which also includes measurements sensitive to charm mixing (see also Sec. 4.3), LHCb finds[50] $\gamma = (65.4^{+3.8}_{-4.2})^\circ$ (see Fig. 6, left), which is the most precise determination from a single experiment and is in excellent agreement with the global CKM fit results.[51,52]

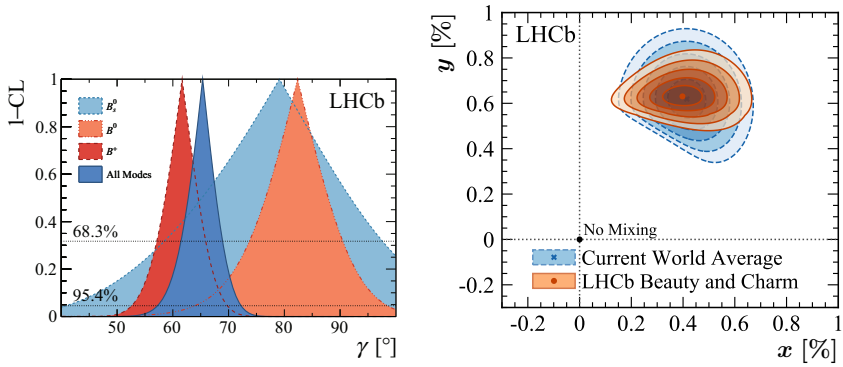

Fig. 6. (Left) One dimensional 1-CL profiles for γ from combinations using inputs from B_s^0, B^0, B^+ mesons and all species together. (Right) Constraints for the charm mixing parameters x and y. Contours are drawn out from 1 to 5 standard deviations.

4.3. *Mixing and CP violation in charm*

At the LHC, the charm cross-section is enormous; e.g., $\sigma(pp \to c\bar{c}X) = (2,369 \pm 192)\,\mu$b at $\sqrt{s} = 13\,\text{TeV}$[53] in the LHCb acceptance. This has allowed LHCb to record the world's largest dataset of charm hadrons to date and to perform numerous high-precision measurements of their production and decay properties. By now, the existence of D^0-$\overline{D}^0$ mixing is well established. The mixing of charm flavour states can be described by two dimensionless parameters, $x \equiv (m_1 - m_2)/\Gamma$ and $y \equiv (\Gamma_1 - \Gamma_2)/2\Gamma$, where $m_i(\Gamma_i)$ is the mass (width) of the appropriate D mass state, and Γ their average decay width. LHCb determined x and y by performing a combination of measurements sensitive to γ and to the charm mixing parameters,[50] thus including, for the first time, inputs from both B- and D-meson decays. Figure 6, right, shows the results for x and y, which are the most precise determinations to date. The precision on y is improved by a factor of two over the current world average.

The discovery of CP violation in charm decays was another important milestone of the LHC flavour program. The size of CP violation in charm decays is expected to be tiny in the SM. However, this might be altered by NP, even if theoretical predictions are difficult to compute reliably due to the presence of low-energy strong-interaction effects. LHCb measured the difference ΔA_{CP} of the time-integrated CP asymmetries in $D^0 \to K^+K^-$ and $D^0 \to \pi^+\pi^-$ decays.[54] The measured value was found to differ from zero by more than five σ, providing the first observation of CP violation in

the decay of charm hadrons and prompting renewed interest in the charm-physics community. The result is consistent with, although in magnitude at the upper end of, SM expectations. More recently, at the 41st ICHEP conference in Bologna, LHCb announced the first evidence for CP violation in a specific charm hadron decay, $D^0 \to \pi^+\pi^-$, with a significance of $3.8\,\sigma$.

4.4. *Exotic hadrons and spectroscopy with heavy flavour*

The LHC is an extremely rich laboratory for the study of heavy-flavour spectroscopy. In 11 years of LHC operation, over 60 hadrons have been discovered by ATLAS, CMS and LHCb; on average about one every two months. This includes exotic states, such as tetraquarks and pentaquarks, as well as many conventional hadrons. A major turning point in exotic baryon spectroscopy was achieved when the LHCb collaboration reported the observation of three significant pentaquark states, $P_c(4312)^+$, $P_c(4440)^+$, and $P_c(4457)^+$, decaying to $J/\psi p$ in $\Lambda_b^0 \to J/\psi p K^-$ decays.[55] Since then many other exotic hadrons have been observed by LHCb. These include, for example, fully heavy tetraquarks with hidden flavour, such as the $X(6900)$ discovered in the $J/\psi J/\psi$ mass distribution,[56] or doubly flavoured tetraquarks, such as the narrow doubly charmed T_{cc}^+ state decaying to $D^0 D^0 \pi^+$.[57] These discoveries have generated a lot of interest and the development of QCD-motivated models. However, no single theoretical model (e.g., based on loosely bound molecules or on tightly bound compact objects) can accommodate all of them, exposing our lack of understanding of hadronic states.

5. Top physics

The top quark is the heaviest known elementary particle and the only quark that decays before it hadronizes. The LHC, with its large collision energy and very high instantaneous luminosity makes it a top quark factory: over half a billion top quarks will have been produced during run 2. This large sample of top quarks allows for high precision measurements of many of its properties, for the measurement of rare production modes, and for searches for very rare decays.

The precise measurement of the top quark mass is an important goal of the LHC experiments as it allows for self-consistency tests of the SM when combined with other precision electroweak measurements. Direct and indirect measurements of the top quark mass have been performed: direct

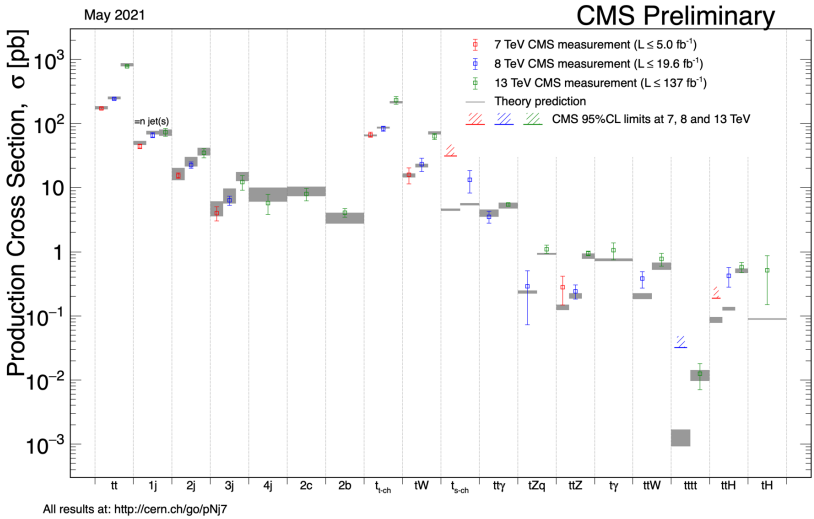

Fig. 7. Summary of several top-quark related production cross section measurements by CMS, compared to the corresponding theoretical expectations.[60]

measurements reconstruct the top quark mass from its decay products while the mass can also be measured indirectly using other measurements that exhibit a mass dependence, like the production cross section. The best single measurement of the top quark mass has been obtained by the CMS experiment and yields a value of 171.77 ± 0.38 GeV.[58]

The main top quark production process at the LHC is pair production. Top quarks can also be produced singly, in association with other particles like photons, W bosons, or Z bosons. Evidence of the rare production of four top quarks has also been reported by the ATLAS Experiment.[59] Figure 7 shows various measured top production processes compared to SM predictions. Overall, very good agreement is observed with theoretical predictions.

The very large sample of top quarks produced by the LHC allows for unprecedented sensitivity to extremely rare decays of the top quark, including FCNC decays. Given that some of these rare decays are not predicted by the SM to be observable at the LHC, an observation would signal NP. Figure 8 displays the limits in the branching fraction obtained for a wide variety of FCNC searches.[61] No significant excess of events has been observed up until now and some of the branching ratio limits extend to 10^{-5} at the end of run 2.

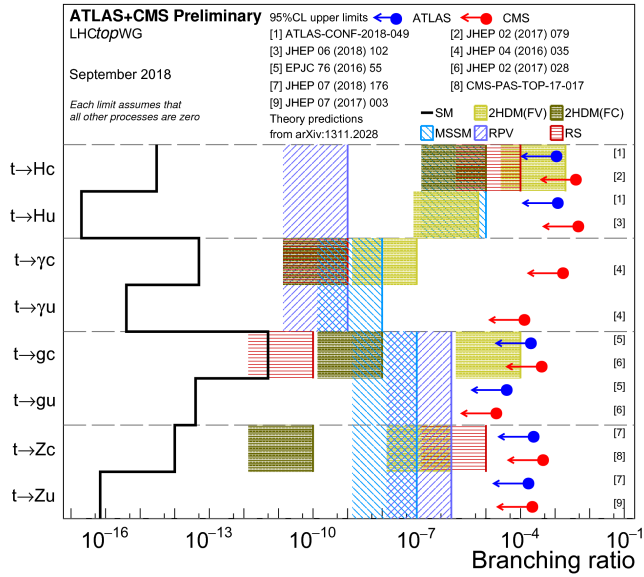

Fig. 8. Summary of the current 95% confidence level observed limits on the branching ratios of the top quark decays via FCNC to a quark and a neutral boson $t \to X_q$ ($X = g$, Z, γ or H; $q = u$ or c) by the ATLAS and CMS collaborations compared to several NP models.[61] Each limit assumes that all other FCNC processes vanish.

6. The Higgs boson

Since the 2012 discovery by the ATLAS and CMS experiments of a new particle with properties consistent with those of the SM Higgs boson, our understanding of this particle has improved significantly. Using the data collected during run 1, the experiments demonstrated that the spin of the discovered particle is consistent with zero. Alternate spin-1 and spin-2 hypotheses were also tested and were excluded at a high level of confidence. In addition, studies of its CP properties were consistent with a CP-even state as predicted by the SM. These detailed studies of the Higgs boson continued during run 2, where 30 times more Higgs bosons are predicted to have been produced compared to the dataset available at the time of discovery. This much larger dataset allowed for precision measurements of the Higgs boson mass, of its production and decay rates, and of its couplings. The Higgs boson mass is not predicted in the SM and must be measured to obtain production and decay rate predictions. The mass has now been measured by the ATLAS and CMS experiments with an uncertainty of

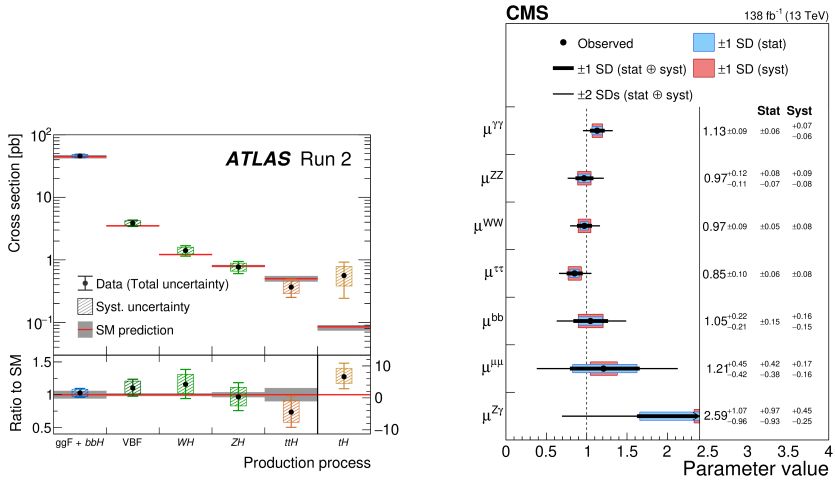

Fig. 9. (Left) Observed and predicted Higgs boson production cross sections from the ATLAS experiment.[65] Higgs boson production processes are measured assuming SM values for the decay branching fractions. (Right) CMS signal strength parameters extracted for decay channels (μ_f) assuming the SM production cross sections.[66] The thick (thin) black lines indicate the 1 (2) σ confidence intervals, with the systematic and statistical components of the 1 σ interval indicated by the red and blue bands, respectively. The vertical dashed line at unity represents the predicted SM values.

approximately 0.1%. The most precise measurement of the Higgs boson mass has been obtained by CMS and yields a value of 125.38 ± 0.14 GeV.[62] The natural width of the Higgs boson at a mass of 125 GeV is predicted to be 4.1 MeV[63] and while a direct measurement of that width is not possible at the LHC, indirect measurements performed under certain assumptions have been carried out. The most precise published measurement is obtained by using the ratio of on-shell to off-shell production cross sections and yields a value of $3.2^{+2.4}_{-1.7}$ MeV.[64]

The main production and decay processes of the Higgs boson have been investigated using the run 2 dataset and measurements are shown in Fig. 9 for the production[65] and decay rates,[66] respectively. Overall, a very good agreement with SM predictions is observed. The results of these measurements can be combined in order to extract the couplings of individual particles to the Higgs boson. The results of such a fit by the ATLAS experiment[65] is shown in Fig. 10, left.

One of the main physics goals of the future High-Luminosity LHC will be to study the shape of the Higgs field potential through the measurement

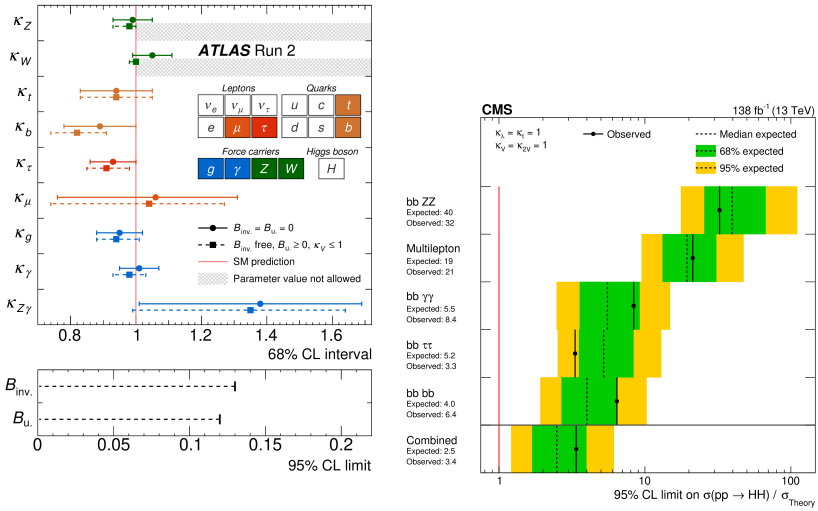

Fig. 10. (Left) Reduced coupling strength modifiers and their uncertainties per particle type with effective photon, $Z\gamma$ and gluon couplings.[65] The horizontal bars on each point denote the 68% confidence interval. The scenario where $B_{\text{inv.}} = B_{\text{u.}} = 0$ is assumed is shown as solid lines with circle markers. ($B_{\text{inv.}}$ and $B_{\text{u.}}$ denote branching fractions for decays to invisible and other undetected particles.) The p-value for compatibility with the SM prediction is 61% in this case. The scenario where $B_{\text{inv.}}$ and $B_{\text{u.}}$ are allowed to contribute to the total Higgs boson decay width while assuming that $\kappa_V \leq 1$ and $B_{\text{u.}} \leq 0$ is shown as dashed lines with square markers. The lower panel shows the 95% CL upper limits on $B_{\text{inv.}}$ and $B_{\text{u.}}$. (Right) The expected and observed limits on the ratio of experimentally estimated production cross section and the expectation from the SM in searches using different final states and their combination.[66] The search modes are ordered, from upper to lower, by their expected sensitivities from the least to the most sensitive. The overall combination of all searches is shown by the lowest entry.

of the self-coupling of the Higgs boson. This is done by searching for double Higgs production in a variety of final states determined by the Higgs decay modes. With the run 2 dataset, the sensitivity that has been achieved by ATLAS and CMS has exceeded previous projections. The current limits at 95% confidence level from the CMS collaboration[66] are shown in Fig. 10 (right), and the associated 95% limits on the Higgs self-coupling parameter κ_λ bound the range between -1.24 and 6.49.

7. Direct Searches for New Physics

Searches for NP is one of the main topics of the LHC experimental program. In this section focus is on the direct observation of new particles and

interactions at the LHC. The palette of proposed theoretical scenarios for NP is very rich. Examples are supersymmetry, extra dimensions, quantum black holes, vector-like fermions, new gauge bosons, hidden valley phenomena, leptoquarks, heavy neutrinos, particles from the dark side,... Over the last years the community got, at times, confronted with suggestions of potential signals, creating excitement for a short time. One such occasion was a putative new resonance at a mass of 750 GeV in early 2016, observed with a significance of about 3σ in the first data collected at 13 TeV. This led to a flurry of about 500 theoretical papers within less than six months, up and until that it became clear that additional collected data did not confirm it. To date no evidence for any new particles or new interactions has been conclusively established, alas. In the following we will discuss some examples of conducted searches.

7.1. *Supersymmetry*

Supersymmetry (SUSY) is a concept proposed to solve the hierarchy problem, provide DM candidates, set the stage for the grand unification of all forces, and more. At the start of the LHC it was anticipated that SUSY was just around the corner waiting to deliver spectacular signals of decays of heavy new particles in the detectors. Interesting events were found, but not more than what could be explained by SM background processes. If realized in Nature, the LHC could have found ample evidence by now, unless the mass scales involved are larger than present sensitivities or the signatures difficult to isolate.

SUSY searches are conducted in ATLAS and CMS by exploring regions of signatures that correspond to decays of heavy new (SUSY) particles. There is a large variety of possible searches, which typically include signatures like large missing transverse momentum, corresponding to an escaping invisible stable lightest SUSY particles (LSP), isolated leptons and a number of jets. Backgrounds are estimated with data-driven techniques, and an optimal sensitivity to a signal is often obtained making use of machine learning techniques. So far no significant excess has been found in any of the SUSY analyses, and the results are mostly interpreted in terms of limits on so called Simplified ModelS (SMS),[67,68] a language designed to facilitate the interpretation of the experimental results. In Fig. 11, SMS limits are shown for searches for gluinos and for light quark SUSY partners versus the neutralino mass, excluding masses up to about 2 TeV.

Despite the null results so far, SUSY will remain a strong candidate for

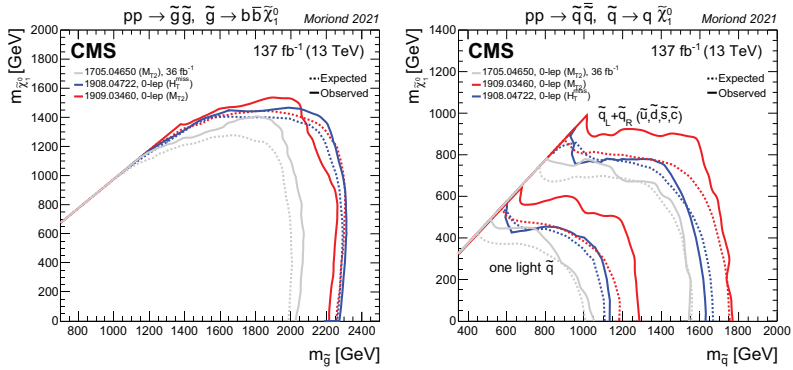

Fig. 11. (Left) Mass limits for a simplified model of gluino pair production with gluino decays to pairs of bottom quarks and the LSP. (Right) Mass limits for a simplified model of first or second generation squark pair production with squark decays to a quark and the LSP. The solid (dashed) lines correspond to the observed (median expected) limits. Limits are shown for two scenarios: production of eight degenerate squarks, or of a single squark. From Ref. 69.

searches for NP, but the preferred region is starting to narrow down.

7.2. *Dark Matter*

The nature of dark matter is one of the most intriguing open questions in fundamental physics today. If dark matter is caused by a particle, the SM does not deliver a candidate to play that role. If dark matter has more than only gravitational interactions, e.g., a weak interaction with the SM particles, it can be produced in the high energy collisions at the LHC. Produced dark matter would not be detected directly in the experiments, but via a large missing transverse momentum. These searches rely on the presence of additional initial state radiation, such as jets, gauge bosons, heavy quarks, etc. If the new interaction with the SM particles is as expected mediated by a new boson also interactions with only incoming and outgoing SM particles contain information for the search. To date, no evidence of dark matter production at the LHC has been observed. Figure 12 shows present limits in interaction strength and dark matter mass, compared to underground direct dark matter experiment limits.

Searches for dark matter are also conducted in other channels such as invisible Higgs decays, light dark matter ($m_{\mathrm{DM}} < 1$ GeV), axion/axion-like particles and more. Interestingly, a decommissioned LHC magnet has been used by the CAST experiment to track the sun for axion to photon

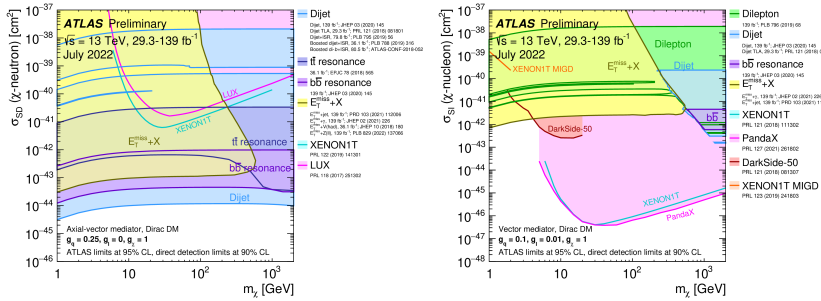

Fig. 12. A comparison of the inferred limits with the constraints from direct-detection experiments on the (Left) spin-dependent WIMP-neutron cross section and (Right) spin-independent WIMP-nucleus cross section in the context of the (Left) leptophobic axial-vector or (Right) vector mediator simplified model. Each shaded region represents the union of the exclusion contours of the individual analyses listed in the legend, where more than one result contributes. The results from this analysis are compared with limits from direct-detection experiments. LHC limits are shown at 95% CL and direct-detection limits at 90% CL. The comparison is valid solely in the context of this model, assuming a mediator width fixed by the dark matter mass, a DM coupling $g_\chi = 1$, quark coupling $g_q = 0.25$, and no coupling to leptons. LHC searches and direct-detection experiments exclude the shaded areas. Exclusions of smaller scattering cross sections do not imply that larger scattering cross sections are also excluded. The resonance and E_T^{miss}+X exclusion regions represent the union of exclusions from all analyses of that type. From Ref. 71.

conversions in the strong $\sim$ 9T magnetic field over a length of 9.26 m, and has produced world-leading limits.[70] The hunt for dark matter will continue in future LHC runs!

7.3. *Long Lived Particles*

The absence of clear evidence for any sign of New Physics at the LHC so far has recently led to an expansion in new search directions. One such new direction is the search for particles that are stable long enough to allow them to travel macroscopic distances, from at least a few mm to several meters or even much further. These so called long-lived particles (LLPs) require new reconstruction methods and search techniques.[72] Many searches for LLPs have been conducted in recent years. A few examples from ATLAS, CMS and LHCb are searches for heavy neutral leptons,[73] displaced muons,[74] displaced jets,[75,76] multicharged particles,[77] disappearing tracks[78] and R-Parity Violating SUSY decays.[79] Figure 13, left, shows limits from searches for a Higgs boson decaying into low mass LLPs in various decay channels.

A particular search is that for magnetic monopoles, i.e., particles that

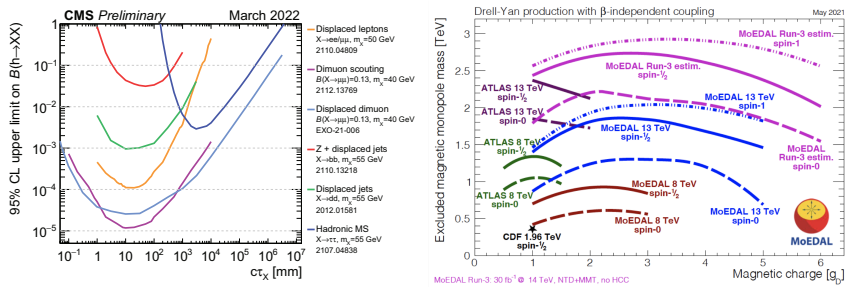

Fig. 13. (Left) The 95% CL observed exclusion limit from different CMS hadronic long-lived particle analyses on the branching fraction of the SM Higgs boson, h, to two neutral long-lived particles, X, shown as a function of the long-lived particle's proper lifetime. (Right) Magnetic monopole mass limits from CDF,[80] ATLAS[81,82] and MoEDAL searches[83–85] as a function of magnetic charge for various spins, assuming Drell-Yan pair- production mechanism and a beta-independent coupling. The MoEDAL projection for LHC run 3 assuming a 30 fb^{-1} integrated luminosity and combined NTD and MMT data is superimposed.

carry a hypothetical magnetic charge, which is quantized and, according to Dirac, one magnetic charge unit corresponds to 137/2 times the electric charge unit of the electron. Such studies can be conducted by the LHC general detectors. However, the largest span in the magnetic charge versus mass space is covered by the MoEDAL experiment. MoEDAL is specially tailored for searches of exotic long-lived particles with a larger than elementary charge. This experiment consists of layers of plastic sheets through which the highly charged particles will literally "burn their way" (Nuclear Track Detector NTD), and aluminum rods that will slow down and stop the stable monopoles and can be unveiled by tracking the rods through a precision SQUID (Magnetic Monopole Tagger MMT). Figure 13, right, shows a summary of the limits set by CDF, ATLAS and MoEDAL.

Direct searches for BSM physics will continue to be a high activity of research at the LHC in the next 10–20 years; it needs really only one convincing significant deviation from the SM or a new observed particle to lead the way in the New Physics world.

References

1. G. Aad et al., The ATLAS Experiment at the CERN Large Hadron Collider, *JINST*. **3**, S08003 (2008). doi: 10.1088/1748-0221/3/08/S08003.
2. S. Chatrchyan et al., The CMS Experiment at the CERN LHC, *JINST*. **3**, S08004 (2008). doi: 10.1088/1748-0221/3/08/S08004.

3. LHCb collaboration, A.A. Alves Jr. et al., The LHCb Detector at the LHC, *JINST.* **3**, S08005 (2008). doi: 10.1088/1748-0221/3/08/S08005.
4. K. Aamodt et al., The ALICE experiment at the CERN LHC, *JINST.* **3**, S08002 (2008). doi: 10.1088/1748-0221/3/08/S08002.
5. G. Anelli et al., The TOTEM experiment at the CERN Large Hadron Collider, *JINST.* **3**, S08007 (2008). doi: 10.1088/1748-0221/3/08/S08007.
6. O. Adriani et al., The LHCf detector at the CERN Large Hadron Collider, *JINST.* **3**, S08006 (2008). doi: 10.1088/1748-0221/3/08/S08006.
7. B. Acharya et al., The Physics Programme Of The MoEDAL Experiment At The LHC, *Int. J. Mod. Phys. A.* **29**, 1430050 (2014). doi: 10.1142/S0217751X14300506.
8. G. Antchev et al., First measurement of elastic, inelastic and total cross-section at $\sqrt{s} = 13$ TeV by TOTEM and overview of cross-section data at LHC energies, *Eur. Phys. J. C.* **79** (2), 103 (2019). doi: 10.1140/epjc/s10052-019-6567-0.
9. A. Tumasyan et al., First search for exclusive diphoton production at high mass with tagged protons in proton-proton collisions at $\sqrt{s} = 13$ TeV, *Phys. Rev. Lett.* **129**, 011801 (2022). doi: 10.1103/PhysRevLett.129.011801.
10. G. Antchev et al., Evidence for non-exponential elastic proton–proton differential cross-section at low —t— and $\sqrt{s} = 8$ TeV by TOTEM, *Nucl. Phys. B.* **899**, 527–546 (2015). doi: 10.1016/j.nuclphysb.2015.08.010.
11. V. M. Abazov et al., Odderon Exchange from Elastic Scattering Differences between pp and $p\bar{p}$ Data at 1.96 TeV and from pp Forward Scattering Measurements, *Phys. Rev. Lett.* **127** (6), 062003 (2021). doi: 10.1103/PhysRevLett.127.062003.
12. A. Tiberio et al., Very-forward π^0 production cross section in proton-proton collisions at $\sqrt{s} = 13$ TeV measured with the LHCf experiment, *PoS.* **ICRC2021**, 386 (2021). doi: 10.22323/1.395.0386.
13. O. Adriani et al., Measurement of energy flow, cross section and average inelasticity of forward neutrons produced in $\sqrt{s} = 13$ TeV proton-proton collisions with the LHCf Arm2 detector, *JHEP.* **07**, 016 (2020). doi: 10.1007/JHEP07(2020)016.
14. K. Aamodt et al., First proton-proton collisions at the LHC as observed with the ALICE detector: Measurement of the charged particle pseudorapidity density at s**(1/2) = 900-GeV, *Eur. Phys. J. C.* **65**, 111–125 (2010). doi: 10.1140/epjc/s10052-009-1227-4.
15. V. Khachatryan et al., Transverse Momentum and Pseudorapidity Distributions of Charged Hadrons in pp Collisions at $\sqrt{s} = 0.9$ and 2.36 TeV, *JHEP.* **02**, 041 (2010). doi: 10.1007/JHEP02(2010)041.
16. G. Aad et al., Charged-particle multiplicities in pp interactions at $\sqrt{s} =$ 900 GeV measured with the ATLAS detector at the LHC, *Phys. Lett. B.* **688**, 21–42 (2010). doi: 10.1016/j.physletb.2010.03.064.
17. LHCb collaboration, R. Aaij et al., Prompt K_s^0 production in pp collisions at $\sqrt{s} = 0.9$ TeV, *Phys. Lett. B.* **693**, 69–80 (2010). doi: 10.1016/j.physletb.2010.08.055.
18. A. Tumasyan et al., Measurement and QCD analysis of double-differential

inclusive jet cross sections in proton-proton collisions at $\sqrt{s} = 13$ TeV, *JHEP*. **02**, 142 (2022). doi: 10.1007/JHEP02(2022)142.

19. M. Aaboud et al., Measurement of inclusive jet and dijet cross-sections in proton-proton collisions at $\sqrt{s} = 13$ TeV with the ATLAS detector, *JHEP*. **05**, 195 (2018). doi: 10.1007/JHEP05(2018)195.
20. R. D. Ball et al., The PDF4LHC21 combination of global PDF fits for the LHC Run III (3, 2022).
21. D. d'Enterria and A. Poldaru, Extraction of the strong coupling $\alpha_s(\mathrm{m}_Z)$ from a combined NNLO analysis of inclusive electroweak boson cross sections at hadron colliders, *JHEP*. **06**, 016 (2020). doi: 10.1007/JHEP06(2020)016.
22. M. Aaboud et al., Measurement of the W-boson mass in pp collisions at $\sqrt{s} = 7$ TeV with the ATLAS detector, *Eur. Phys. J. C*. **78** (2), 110 (2018). doi: 10.1140/epjc/s10052-017-5475-4. [Erratum: Eur. Phys. J. C 78, 898 (2018)].
23. LHCb collaboration, R. Aaij et al., Measurement of the W boson mass, *JHEP*. **01**, 036 (2022). doi: 10.1007/JHEP01(2022)036.
24. Status of W Mass Measurements. URL `https://cds.cern.ch/record/2806574`.
25. ATLAS Collaboration. Measurement of the effective leptonic weak mixing angle using electron and muon pairs from Z-boson decay in the ATLAS experiment at $\sqrt{s} = 8$ TeV. ATLAS-CONF-2018-037 (2018). URL `https://cds.cern.ch/record/2630340`.
26. A. M. Sirunyan et al., Measurement of the weak mixing angle using the forward-backward asymmetry of Drell-Yan events in pp collisions at 8 TeV, *Eur. Phys. J. C*. **78** (9), 701 (2018). doi: 10.1140/epjc/s10052-018-6148-7.
27. LHCb collaboration, R. Aaij et al., Measurement of the forward-backward asymmetry in $Z/\gamma^* \to \mu^+\mu^-$ decays and determination of the effective weak mixing angle, *JHEP*. **11**, 190 (2015). doi: 10.1007/JHEP11(2015)190.
28. ATLAS SM Public Results. URL `https://atlas.web.cern.ch/Atlas/GROUPS/PHYSICS/PUBNOTES/ATL-PHYS-PUB-2022-009/`.
29. C. Bobeth, M. Gorbahn, T. Hermann, M. Misiak, E. Stamou, and M. Steinhauser, $B_{s,d} \to l^+l^-$ in the Standard Model with reduced theoretical uncertainty, *Phys. Rev. Lett.* **112**, 101801 (2014). doi: 10.1103/PhysRevLett.112.101801.
30. M. Beneke, C. Bobeth, and R. Szafron, Power-enhanced leading-logarithmic QED corrections to $B_q \to \mu^+\mu^-$, *JHEP*. **10**, 232 (2019). doi: 10.1007/JHEP10(2019)232.
31. ATLAS, CMS, LHCb collaborations, Combination of the ATLAS, CMS and LHCb results on the $B^0_{(s)} \to \mu^+\mu^-$ decays (2020). LHCb-CONF-2020-002, ATLAS-CONF-2020-049, CMS-PAS-BPH-20-003.
32. CMS collaboration, Measurement of $B^0_s \to \mu^+\mu^-$ decay properties and search for the $B^0 \to \mu^+\mu^-$ decay in proton-proton collisions at $\sqrt{s} = 13$ TeV (2022). URL `https://cds.cern.ch/record/2815334`.
33. LHCb collaboration, R. Aaij et al., Differential branching fractions and isospin asymmetries of $B \to K^{(*)}\mu^+\mu^-$ decays, *JHEP*. **06**, 133 (2014). doi: 10.1007/JHEP06(2014)133.

34. LHCb collaboration, R. Aaij et al., Measurements of the S-wave fraction in $B^0 \to K^+\pi^-\mu^+\mu^-$ decays and the $B^0 \to K^*(892)^0\mu^+\mu^-$ differential branching fraction, *JHEP.* **11**, 047 (2016). doi: 10.1007/JHEP11(2016)047.
35. LHCb collaboration, R. Aaij et al., Differential branching fraction and angular analysis of $\Lambda_b \to \Lambda\mu^+\mu^-$ decays, *JHEP.* **06**, 115 (2015). doi: 10.1007/JHEP06(2015)115.
36. LHCb collaboration, R. Aaij et al., Branching fraction measurements of the rare $B_s^0 \to \phi\mu^+\mu^-$ and $B_s^0 \to f_2'(1525)\mu^+\mu^-$ decays, *Phys. Rev. Lett.* **127**, 151801 (2021). doi: 10.1103/PhysRevLett.127.151801.
37. A. Bharucha, D. M. Straub, and R. Zwicky, $B \to V\ell^+\ell^-$ in the Standard Model from light-cone sum rules, *JHEP.* **2016** (8), 1–64 (2016).
38. W. Altmannshofer and D. M. Straub, New physics in $b \to s$ transitions after LHC run 1, *The European Physical Journal C.* **75** (8), 1–30 (2015).
39. R. R. Horgan, Z. Liu, S. Meinel and M. Wingate, Calculation of $B^0 \to K^{*0}\mu^+\mu^-$ and $B_s^0 \to \phi\mu^+\mu^-$ observables using form factors from lattice QCD, *Phys. Rev. Lett.* **112** (21) (May, 2014). doi: 10.1103/physrevlett.112.212003.
40. LHCb collaboration, R. Aaij et al., Measurement of *CP*-averaged observables in the $B^0 \to K^{*0}\mu^+\mu^-$ decays decay, *Phys. Rev. Lett.* **125**, 011802 (2020). doi: 10.1103/PhysRevLett.125.011802.
41. S. Descotes-Genon, L. Hofer, J. Matias and J. Virto, On the impact of power corrections in the prediction of $B \to K^*\mu^+\mu^-$ observables, *JHEP.* **2014** (12), 125 (2014). doi: 10.1007/JHEP12(2014)125.
42. T. M. A. Khodjamirian, A. Pivovarov, and Y.-M. Wang, Charm-loop effect in $B \to K^{(*)}\ell^+\ell^-$ and $B \to K^*\gamma$, *JHEP.* **2010** (9) (Sep, 2010). doi: 10.1007/jhep09(2010)089.
43. S. Descotes-Genon, J. Matias, M. Ramon and J. Virto, Implications from clean observables for the binned analysis of $B \to K^*\ell\ell$ - at large recoil, *JHEP.* **2013** (1) (Jan, 2013). doi: 10.1007/jhep01(2013)048.
44. LHCb collaboration, R. Aaij et al., Test of lepton universality in beauty-quark decays, *Nature Physics.* **18** (3), 277–282 (2022).
45. LHCb collaboration, R. Aaij et al., Test of lepton universality with $B^0 \to K^{*0}\ell^+\ell^-$ decays, *JHEP.* **08**, 055 (2017). doi: 10.1007/JHEP08(2017)055.
46. Y. Amhis et al., Averages of b-hadron, c-hadron, and τ-lepton properties as of 2021. URL `https://arxiv.org/abs/2206.07501` (2022).
47. LHCb collaboration, R. Aaij et al., Measurement of lepton universality parameters in $B^+ \to K^+\ell^+\ell^-$ and $B^0 \to K^{*0}\ell^+\ell^-$ decays (2022). Submitted to Phys. Rev. D.
48. LHCb collaboration, R. Aaij et al., Test of lepton universality in $b \to s\ell^+\ell^-$ decays (2022). Submitted to Phys. Rev. Lett.
49. LHCb collaboration, R. Aaij et al., Measurement of the CKM angle γ in $B^\pm \to DK^\pm$ and $B^\pm \to D\pi^\pm$ decays with $D \to K_s^0h^+h^-$, *JHEP.* **2021** (2) (Feb, 2021). doi: 10.1007/jhep02(2021)169.
50. LHCb collaboration, R. Aaij et al., Simultaneous determination of CKM angle γ and charm mixing parameters, *JHEP.* **2021** (12) (Dec, 2021). doi: 10.1007/jhep12(2021)141.

51. CKMfitter group, J. Charles et al., Current status of the standard model CKM fit and constraints on $\Delta F = 2$ new physics, *Phys. Rev. D.* **91** (7) (Apr, 2015). doi: 10.1103/physrevd.91.073007. Updated results and plots available at http://ckmfitter.in2p3.fr/.
52. UTfit collaboration, M. Bona et al., The unitarity triangle fit in the standard model and hadronic parameters from lattice QCD: a reappraisal after the measurements of Δm_s and $BR(B \to \tau\nu_\tau)$, *JHEP.* **2006** (10), 081–081 (Oct, 2006). doi: 10.1088/1126-6708/2006/10/081. Updated results and plots available at http://www.utfit.org/.
53. LHCb collaboration, R. Aaij et al., Measurements of prompt charm production cross-sections in pp collisions at $\sqrt{s} = 13$ TeV, *JHEP.* **03**, 159 (2016). doi: 10.1007/JHEP03(2016)159.
54. LHCb collaboration, R. Aaij et al., Observation of CP Violation in Charm Decays, *Phys. Rev. Lett.* **122** (21) (May, 2019). doi: 10.1103/physrevlett.122.211803.
55. LHCb collaboration, R. Aaij et al., Observation of a Narrow Pentaquark State, $P_c(4312)^+$, and of two-peak structure of the $P_c(4450)^+$, *Phys. Rev. Lett.* **122** (22) (Jun, 2019). doi: 10.1103/physrevlett.122.222001.
56. LHCb collaboration, R. Aaij et al., Observation of structure in the J/ψ-pair mass spectrum, *Science Bulletin.* **65** (23), 1983–1993 (2020). ISSN 2095-9273. doi: https://doi.org/10.1016/j.scib.2020.08.032.
57. LHCb collaboration, R. Aaij et al., Study of the doubly charmed tetraquark T_{cc}^+, *Nature Communications.* **13** (1), 3351 (2022).
58. CMS collaboration, A profile likelihood approach to measure the top quark mass in the lepton+jets channel at $\sqrt{s} = 13$ TeV (2022). URL `https://cds.cern.ch/record/2806509`.
59. G. Aad et al., Measurement of the $\mathrm{t\bar{t}t\bar{t}}$ production cross section in pp collisions at $\sqrt{s} = 13$ TeV with the ATLAS detector, *JHEP.* **11**, 118 (2021). doi: 10.1007/JHEP11(2021)118.
60. CMS Top Quark Cross Sections Measurements. URL `https://twiki.cern.ch/twiki/pub/CMSPublic/PhysicsResultsCombined/`.
61. Flavour Changing Neutral Current Decays. URL `https://twiki.cern.ch/twiki/bin/view/LHCPhysics/LHCTopWGSummaryPlots/`.
62. CMS Collaboration, A measurement of the Higgs boson mass in the diphoton decay channel, *Phys. Lett. B.* **805**, 135425 (Jun, 2020). doi: 10.1016/j.physletb.2020.135425. URL `https://doi.org/10.1016%2Fj.physletb.2020.135425`.
63. CERN. Cern yellow reports: Monographs, vol. 2 (2017): Handbook of lhc higgs cross sections: 4. deciphering the nature of the higgs sector. URL `https://e-publishing.cern.ch/index.php/CYRM/issue/view/32` (2017).
64. CMS Collaboration, Measurement of the higgs boson width and evidence of its off-shell contributions to zz production, *Nature Physics.* **19**, 1329–1334 (2022).
65. A detailed map of Higgs boson interactions by the ATLAS experiment ten years after the discovery, *Nature.* **607** (7917), 52–59 (Jul, 2022). doi: 10.1038/s41586-022-04893-w.

66. A portrait of the Higgs boson by the CMS experiment ten years after the discovery, *Nature.* **607** (7917), 60–68 (Jul, 2022). doi: 10.1038/s41586-022-04892-x.
67. J. Alwall, P. Schuster, and N. Toro, Simplified Models for a First Characterization of New Physics at the LHC, *Phys. Rev. D.* **79**, 075020 (2009). doi: 10.1103/PhysRevD.79.075020.
68. D. Alves, Simplified Models for LHC New Physics Searches, *J. Phys. G.* **39**, 105005 (2012). doi: 10.1088/0954-3899/39/10/105005.
69. CMS SUSY Public Results. URL `https://twiki.cern.ch/twiki/bin/view/CMSPublic/PhysicsResultsSUS`.
70. V. Anastassopoulos et al., New CAST Limit on the Axion-Photon Interaction, *Nature Phys.* **13**, 584–590 (2017). doi: 10.1038/nphys4109.
71. ATLAS EXO Public Results. URL `https://atlas.web.cern.ch/Atlas/GROUPS/PHYSICS/PUBNOTES/ATL-PHYS-PUB-2021-045/`.
72. J. Alimena et al., Searching for long-lived particles beyond the Standard Model at the Large Hadron Collider, *J. Phys. G.* **47** (9), 090501 (2020). doi: 10.1088/1361-6471/ab4574.
73. A. Tumasyan et al., Search for long-lived heavy neutral leptons with displaced vertices in proton-proton collisions at $\sqrt{s}$ =13 TeV, *JHEP.* **07**, 081 (2022). doi: 10.1007/JHEP07(2022)081.
74. A. Tumasyan et al., Search for long-lived particles decaying into muon pairs in proton-proton collisions at $\sqrt{s} = 13$ TeV collected with a dedicated high-rate data stream, *JHEP.* **04**, 062 (2022). doi: 10.1007/JHEP04(2022)062.
75. A. M. Sirunyan et al., Search for long-lived particles decaying to jets with displaced vertices in proton-proton collisions at $\sqrt{s} = 13$ TeV, *Phys. Rev. D.* **104** (5), 052011 (2021). doi: 10.1103/PhysRevD.104.052011.
76. G. Aad et al., Search for neutral long-lived particles in pp collisions at $\sqrt{s} =$ 13 TeV that decay into displaced hadronic jets in the ATLAS calorimeter (3, 2022).
77. M. Aaboud et al., Search for heavy long-lived multicharged particles in proton-proton collisions at $\sqrt{s} = 13$ TeV using the ATLAS detector, *Phys. Rev. D.* **99** (5), 052003 (2019). doi: 10.1103/PhysRevD.99.052003.
78. G. Aad et al., Search for long-lived charginos based on a disappearing-track signature using 136 fb^{-1} of pp collisions at $\sqrt{s} = 13$ TeV with the ATLAS detector (1, 2022).
79. R. Aaij et al., Search for long-lived particles decaying to $e^{\pm}\mu^{\mp}\nu$, *Eur. Phys. J. C.* **81** (3), 261 (2021). doi: 10.1140/epjc/s10052-021-08994-0.
80. A. Abulencia et al., Direct search for Dirac magnetic monopoles in $p\bar{p}$ collisions at $\sqrt{s} = 1.96$ TeV, *Phys. Rev. Lett.* **96**, 201801 (2006). doi: 10.1103/PhysRevLett.96.201801.
81. G. Aad et al., Search for magnetic monopoles and stable particles with high electric charges in 8 TeV pp collisions with the ATLAS detector, *Phys. Rev. D.* **93** (5), 052009 (2016). doi: 10.1103/PhysRevD.93.052009.
82. G. Aad et al., Search for Magnetic Monopoles and Stable High-Electric-Charge Objects in 13 Tev Proton-Proton Collisions with the ATLAS Detector, *Phys. Rev. Lett.* **124** (3), 031802 (2020). doi: 10.1103/PhysRevLett.124.031802.

83. B. Acharya et al., Search for magnetic monopoles with the MoEDAL prototype trapping detector in 8 TeV proton-proton collisions at the LHC, *JHEP*. **08**, 067 (2016). doi: 10.1007/JHEP08(2016)067.
84. B. Acharya et al., Search for magnetic monopoles with the MoEDAL forward trapping detector in 2.11 fb^{-1} of 13 TeV proton-proton collisions at the LHC, *Phys. Lett. B.* **782**, 510–516 (2018). doi: 10.1016/j.physletb.2018.05.069.
85. B. Acharya et al., Magnetic Monopole Search with the Full MoEDAL Trapping Detector in 13 TeV pp Collisions Interpreted in Photon-Fusion and Drell-Yan Production, *Phys. Rev. Lett.* **123** (2), 021802 (2019). doi: 10.1103/PhysRevLett.123.021802.